Chem. Mater. **2005,** *17,* 6369−6380 6369

Coexistence of Spin-Canting, Metamagnetism, and Spin-Flop in a (4,4) Layered Manganese Azide Polymer

Xin-Yi Wang,[†] Lu Wang,[†] Zhe-Ming Wang,[†] Gang Su,[‡] and Song Gao*,[†]

State Key Laboratory of Rare Earth Materials Chemistry and Applications & PKU−HKU Joint Laboratory on Rare Earth Materials and Bioinorganic Chemistry, College of Chemistry and Molecular Engineering, Peking University, Beijing 100871, People's Republic of China, and College of Physical Sciences, Graduate School of the Chinese Academy of Sciences, P.O. Box 4588, Beijing 100049, People's Republic of China

Received September 30, 2005. Revised Manuscript Received October 7, 2005

A novel molecule-based magnetic polymer $Mn(N_3)_2(btr)_2$ **1** (btr = 4,4′-bi-1,2,4-triazole) was synthesized and characterized crystallographically and magnetically. **1** crystallizes in the monoclinic system, space group $P2_1/c$, formula $C_8H_8N_{18}Mn$, with $a = 12.2831(4)$ Å, $b = 6.3680(1)$ Å, $c = 10.2245(3)$ Å, $\beta = 105.064(1)°$, and $Z = 2$. Bridged by end-to-end azides, the Mn^{2+} ions form a two-dimensional layer with (4,4) topology; the layers are further connected to the three-dimensional network by the weak hydrogen bonds between ligands of btr. Magnetic studies on a polycrystalline sample show the existence of strong antiferromagnetic couplings between the adjacent Mn^{2+} ions, and the Neél temperature is $T_N = 23.7$ K. In the ordered state below T_N, detailed investigations on an oriented single-crystal sample of **1** reveal that the hidden spin-canting, metamagnetic transition, and spin-flop transition can appear in different circumstances. The ground state is of an antiferromagnet with hidden spin-canting. An external field applied along the *b* direction parallel to the manganese azide layer can lead to a first-order metamagnetic phase transition, while a spin-flop transition may occur when the field is applied along the *a** direction that is perpendicular to the manganese azide layer. Magnetic phase diagrams in both the $T-H^{a*}$ and the $T-H^{b}$ planes were determined. Possible spin configurations before and after the transitions were proposed. Analyses on the experimental data give the following intrinsic parameters: the intra- and interlayer coupling $J \approx -3.5\ \mathrm{cm}^{-1}$ and $J^{a*} = 6 \times 10^{-4}\ \mathrm{cm}^{-1}$, the anisotropy field $H_A = 0.2$ kOe, the exchange field $H_E = 387.8$ kOe, and the anisotropy parameter $\alpha = 5 \times 10^{-4}$. The small J^{a*} and α show **1** to be a good example of a two-dimensional Heisenberg system.

Introduction

Recent progress of the molecule-based magnetic materials lead to extensive investigations and thorough comprehension on many new fascinating physical phenomena, such as the exotic properties in the single-molecular magnets (SMM),[1] the single-chain magnets (SCM),[2] the geometrically frustrated magnets,[3] etc. Molecule-based magnetic materials also provide good examples to better understand some fundamental phenomena in magnetism (e.g., spin-canting, metamagnetic transition, *s*pin-*f*lop (SF) transition, etc.).[4−12] These three kinds of phenomena are simply sketched in Scheme 1. Spin-canting means the noncollinear spin arrangements on two sublattices of an antiferromagnet.[4−8] If more sublattices with noncollinear *a*nti*f*erromagnetic (AF) spin arrangements are present and a ferromagnetic moment needs not to occur, it is the hidden spin-canting.[8] Metamagnet is the one with net moments aligned in antiparallel by weak AF interactions, which are of secondary importance. A large external field could overwhelm the weak AF interactions and turn the

Scheme 1. Sketches of the Spin-Canting, Metamagnetism and Spin-Flop Phenomena

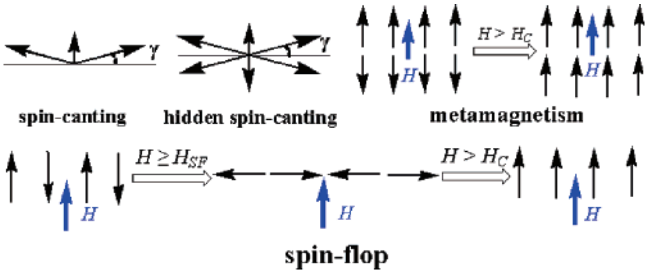

---

* To whom correspondence should be addressed. Fax: +86-10-62751708. Tel.: +86-10-62756320. E-mail: gaosong@pku.edu.cn.

[†] Peking University.

[‡] Graduate School of the Chinese Academy of Sciences.

(1) (a) Sessoli, R.; Gatteschi, D.; Caneschi, A.; Novak, M. A. *Nature* **1993**, *365*, 141−143. (b) Gatteschi, D.; Caneschi, A.; Pardi, L.; Sessoli, R. *Science* **1994**, *265*, 1054−1058. (c) Gatteschi, D.; Sessoli, R. *Angew. Chem. Int. Ed.* **2003**, *42*, 268−297. (d) Tasiopoulos, A. J.; Vinslava, A.; Wernsdorfer, W.; Abboud, K. A.; Christou, G. *Angew. Chem., Int. Ed.* **2004**, *43*, 2117−2121. (For more recent works of Christou, G., one may go to the website http://www.chem.ufl.edu/~christou/group/.)

(2) (a) Glauber, R. J. *J. Math. Phys.* **1963**, *4*, 294−302. (b) Caneschi, A.; Gatteschi, D.; Lalioti, N.; Sangregorio, C.; Sessoli, R.; Venturi, G.; Vindigni, A.; Rettori, A.; Pini, M. G.; Novak, M. A. *Angew. Chem., Int. Ed.* **2001**, *40*, 1760−1763. (c) Clérac, R.; Miyasaka, H.; Yamashita, M.; Coulon, C. *J. Am. Chem. Soc.* **2002**, *124*, 12837−12844. (d) Lescouëzec R.; Vaissermann J.; Ruiz-Pérez C.; Loret F.; Carrasco R.; Julve M.; Verdagurer M.; Draomzee Y.; Gatteschi D.; Wernsdorfer W. *Angew. Chem., Int. Ed.* **2003**, *42*, 1483−1492. (e) Toma, L. M.; Lescouëzec, R.; Lloret, F.; Julve, M.; Vaissermann, J.; Verdaguer, M. *Chem. Commun.* **2003**, 1850−1851. (f) Liu, T. F.; Fu, D.; Gao, S.; Zhang, Y. Z.; Sun, H. L.; Su, G.; Liu, Y. J. *J. Am. Chem. Soc.* **2003**, *125*, 13976−13977. (g) Ferbinteanu, M.; Miyasaka, H.; Wernsdorfer, W.; Nakata, K.; Sugiura, K.; Yamashita, M.; Coulon, C.; Clérac, R. *J. Am. Chem. Soc.* **2005**, *127*, 3090−3099.

10.1021/cm0521830 CCC: $30.25

system to a ferro-, ferri-, or *w*eak-*f*erromagnetic (WF) state, depending on the details of the spin alignments in the AF state.[4,7,9,10] When a spin-flop happens, a field parallel to the easy-axis of an antiferromagnet causes the spins to flop to the direction perpendicular to it.[4,6,8,11,12] Although these three phenomena are mutually different in many aspects, there also exist some common features, such as the important role of the magnetic anisotropy playing in all of them. Generally, a large anisotropy leads to a significant spin-canting through increasing the possible antisymmetric superexchange interaction and may induce a metamagnetic transition in the presence of competing interactions, while a small anisotropy favors the spin-flop transition.[4,11] An appropriate balance between the crystallographic symmetry, the anisotropy, the nearest interactions, and the next-nearest interactions is needed to observe all of these three interesting magnetic phenomena. Therefore, although there are some studies showing the simultaneous presence of two of them (e.g., the spin-canting and spin-flop[6,8] and the spin-canting and metamagnetism[7,8] can be simultaneously observed in one system), few reports concern all three phenomena in one single magnetic system. To the best of our knowledge, a Co^{2+} compound bridged by 1,2,4-trizaole is perhaps the only reported example showing all three phenomena together, although the spin-flop in this system is not traditional.[8d]

Until now, the major emphasis concerning the design of the molecular magnetic materials is still searching for the proper bridges either to efficiently mediate the magnetic interactions or to conveniently construct various interesting structures. Among the most widely used short bridges (such as CN^-, N_3^-, $C_2O_4^{2-}$, $N(CN)_2^-$, etc.), azide is the all-important one, if not the most, because it has the abundant bridging modes and the ability to mediate strong magnetic couplings. Structurally, it can bridge metal ions in the μ_2-1,1 (end-on, EO), μ_2-1,3 (end-to-end, EE), μ_3-1,1,3, or other modes and may magnetically mediate antiferro- or ferromagnetic interactions with different magnitudes, depending on the bridging mode and structural parameters. Furthermore, the different bridging modes may simultaneously exist in the same compound. These features of azide have led to a lot of polymeric architectures with various structures and interesting magnetic behaviors.[2c,7b,10b,10e,13,14] For instance, the two-dimensional networks with metal ions in the nodes of (4,4) squares bridged by EE azide are reported for several compounds.[7b,14] Magnetically, the weak-ferromagnetism,[7b,14a−d] metamagnetism,[7b] and paramagnetism[14e] have been observed in these materials. However, the magnetic characterizations are not fully carried out owing to the lack of suitable big single crystals to perform the experiment.

On the other hand, a number of coligands are used to finely tune the crystal structures and the magnetic properties of the metal−azide systems, including the monocoordinated ligands (e.g., pyridine and its derivatives[13,14a−d]), the chelating ones (e.g., 2,2′-bipyridine[15] and 2,2′-bipyrimidine[16]), the bridging ones (e.g., 4,4′-bipyridine[17] and pyrizine[18]), etc. Here we report that by using a coligand btr (btr = 4,4′-bi-1,2,4-triazole), a new coordination polymer $Mn(N_3)_2(btr)_2$ (**1**) was

---

(3) (a) Ramirez, A. P.; Hayashi, A.; Cava, R. J.; Siddharthan, R.; Shastry, B. S. *Nature* **1999**, *399*, 333−335. (b) Moulton, B.; Lu, J.-J.; Hajndl, R.; Hariharan, S.; Zaworotko, M. J. *Angew. Chem., Int. Ed.* **2002**, *41*, 2821−2824. (c) Atwood, J. L. *Nat. Mater.* **2002**, *1*, 91−92. (d) Grohol, D.; Matan, K.; Cho, J. H.; Lee, S.-H.; Lynn, J. W.; Nocera, D. G.; Lee, Y. S. *Nat. Mater.* **2005**, *4*, 323−328 and references therein.

(4) (a) Carlin, R. L.; Van-Duyneveldt, A. J. *Magnetic Properties of Transition Metal Compounds*; Springer-Verlag: New York, 1977. (b) Carlin, R. L. *Magnetochemistry*; Springer-Verlag: Berlin, 1986.

(5) For examples, see: (a) Rettig, S. J.; Storr, A.; Summers, D. A.; Thompson, R. C.; Trotter J. *J. Am. Chem. Soc.* **1997**, *119*, 8675−8680. (b) Kurmoo, M.; Kepert, C. J. *New J. Chem.* **1998**, 1515−1524. (c) Batten, S. R.; Jenson, P.; Kepert, C. J.; Kurmoo, M.; Moubaraki, B.; Marray, K. S.; Price, D. J. *J. Chem. Soc., Dalton Trans.* **1999**, 2987−2997. (d) Kmety, C. R.; Huang, Q.; Lynn, J. W.; Erwin, R. W.; Manson, J. L.; McCall, S.; Crow, J. E.; Stevenson, K. L.; Miller, J. S.; Epstein, A. J. *Phys. Rev. B* **2000**, *62*, 5576−5588. (e) Mito, M.; Kawae, T.; Takeda, K.; Takagi, S.; Matsushita, Y.; Deguchi, H.; Rawson, J. M.; Palacio, F. *Polyhedron* **2001**, *20*, 1509−1512. (f) Richard-Plouet, M.; Vilminot, S.; Guillot, M.; Kurmoo, M. *Chem. Mater.* **2002**, *14*, 3829−3836. (g) Wang, X. Y.; Gan, L.; Zhang, S. W.; Gao, S. *Inorg. Chem.* **2004**, *43*, 4615−4625. (h) Wang, X. Y.; Wei, H. Y.; Wang, Z. M.; Chen, Z. D.; Gao, S. *Inorg. Chem.* **2005**, *44*, 572−583. (i) Salah, M. B.; Vilminot, S.; Andre, G.; Bouree-Vigneron, F.; Richard-Plouet, M.; Mhiri, T.; Kurmoo, M. *Chem. Mater.* **2005**, *17*, 2612−2621.

(6) (a) Zora, J. A.; Seddon, K. R.; Hitchcock, P. B.; Lowe, C. B.; Shum, D. P.; Carlin, R. L. *Inorg, Chem.* **1990**, *29*, 3302−3308. (b) Lowe, C. B.; Carlin, R. L.; Schultz, A. J.; Loong, C. K. *Inorg. Chem.* **1990**, *29*, 3308−3315. (c) Schlueter, J. A.; Manson, J. L.; Hyzer, K. A.; Geiser, U. *Inorg. Chem.* **2004**, *43*, 4100−4102.

(7) (a) Kurmoo, M.; Kumagai, H.; Green, M. A.; Lovett, B. W.; Blundell, S. J.; Ardavan, A.; Singleton, J. *J. Solid State Chem.* **2001**, *159*, 343−352. (b) Gao, E. Q.; Wang, Z. M.; Yan, C. H. *Chem. Commun.* **2003**, *14*, 1748−1749. (c) Zeng, M. H.; Zhang, W. X.; Sun, X. Z.; Chen, X. M. *Angew. Chem., Int. Ed.* **2005**, *44* (20), 3079−3082.

(8) (a) Herweijer, A.; de Jonge, W. J. M.; Botterman, A. C.; Bongaarts, A. L. M.; Cowen, J. A. *Phys. Rev. B* **1972**, *5*, 4618−4630. (b) Kopinga, K.; van Vlimmeren, Q. A. G.; Bongaarts, A. L. M.; de Jonge, W. J. M. *Physica B+C* **1977**, *86*−*88*, 671−672. (c) Basten, J. A.; van Vlimmeren, Q. A. G.; de Jonge, W. J. M. *Phys. Rev. B* **1978**, *18*, 2179−2184. (d) Engelfriet, D. W.; Groeneveld, W. L.; Groenendijk, H. A.; Smit, J. J.; Nap, G. M. Z. Naturforsch. **1980**, *35A*, 115−128. (e) Carlin, R. L.; Joung, K. O.; van der Bilt, A.; del Adel, H.; O'Connor, C. J.; Sinn, E. *J. Chem. Phys.* **1981**, *75*, 431−439. (f) Tian, Y. Q.; Cai, C. X.; Ren, X. M.; Duan, C, Y.; Xu, Y.; Gao, S.; You, X. Z. *Chem. Eur. J.* **2003**, *9*, 5673−5685.

(9) Stryjewski, E.; Giordano, N. *Adv. Phys.* **1977**, *26*, 487−650.

(10) (a) Kou, H. Z.; Gao, S.; Sun, B. W.; Zhang, J. *Chem. Mater.* **2001**, *13*, 1431−1433. (b) Gao, E. Q.; Yue, Y. F.; Bai, S. Q.; He, Z.; Yan, C. H. *J. Am. Chem. Soc.* **2004**, *126*, 1419−1429. (c) Pereira, C. L. M.; Pedroso, E. F.; Stumpf, H. O.; Novak, M. A.; Ricard, L.; Ruiz-García, R.; Rivière, E.; Journaux, Y. *Angew. Chem., Int. Ed.* **2004**, *43*, 955−958. (d) Toma, L.; Lescoëzec, R.; Vaissermann, J.; Delgado, F. S.; Ruiz-Pérez, C.; Carrasco, R.; Cano, J. Lloret, F.; Julve, M. *Chem. Eur. J.* **2004**, *10*, 6130−6145. (e) Zhang, Y. Z.; Gao, S.; Sun, H. L.; Su, G.; Wang, Z. M.; Zhang, S. W. *Chem. Commun.* **2004**, 1906−1907.

(11) Carlin, R. L.; van Duyneveldt, A. J. *Acc. Chem. Res.* **1980**, *13*, 231−236.

(12) (a) Engelfriet, D. W.; Groeneveld, W. L. Z. Naturforsch. **1978**, *33A*, 845−854. (b) Balanda M.; Falk K.; Griesar K.; Tomkowicz, Z.; Haase W. *J. Magn. Magn. Mater.* **1999**, *205* (1), 14−26. (c) Manson, J. L.; Huang, Q. Zh.; Lynn, J. W.; Koo, H. J.; Whangbo, M. H.; Bateman, R.; Otsuka, T.; Wada, N.; Argylou, D. N.; Miller, J. S. *J. Am. Chem. Soc.* **2001**, *123*, 162−172.

(13) Ribas, J.; Escuer, A.; Monfort, M.; Vicente, R.; Cortés, R.; Lezama, L.; Rojo, T. *Coord. Chem. Rev.* **1999**, *193*−*195*, 1027−1068 and references therein.

(14) (a) Escuer, A.; Vicente, J. R.; Goher, M. A. S.; Mautner, F. A. *Inorg. Chem.* **1995**, *34*, 5707−5708. (b) Escuer, A.; Vicente, J. R.; Goher, M. A. S.; Mautner, F. A. *Inorg. Chem.* **1996**, *35*, 6386-6391. (c) Escuer, A.; Vicente, J. R.; Goher, M. A. S.; Mautner, F. A. *Inorg. Chem.* **1997**, *36*, 3440−3446. (d) Escuer, A.; Vicente, J. R.; Goher, M. A. S.; Mautner, F. A. *J. Chem. Soc., Dalton Trans.* **1997**, 4431−4434. (e) Goher, M. A. S.; Abu-Youssef, M. A. M.; Mautner, F. A.; Vicente, R.; Escuer A. *Eur. J. Inorg. Chem.* **2000**, 1819−1823.

(15) (a) Cortés, R.; Urtiaga, K.; Lezama, L.; Pizarro, J. L.; Goñi, A.; Arriortua, M. I.; Rojo, T. *Inorg. Chem.* **1994**, *33*, 4009−4015. (b) Viau, G.; Lombardi, M. G.; De Munno, G.; Julve, M.; Lloret, F.; Faus, J.; Caneschi, A.; Clemente-Juan, J. M. *Chem. Commun.* **1997**, 1195−1196.

synthesized and characterized structurally and magnetically. It is a two-dimensional compound of the (4,4) topology with the Mn^{2+} ions bridged by EE azide. Magnetic measurements on a polycrystalline sample and a well-shaped single crystal show that **1** undergoes a transition from paramagnetism to a long-range ordering state at the Neél temperature $T_N = 23.7$ K. Careful investigation in the ordered state reveals the coexistence of the above-mentioned three interesting phenomena (spin-canting, metamagnetism, and spin-flop) in this molecular system. On the basis of a series of measurements, we determined the magnetic phase diagrams in both the $T-H^{a*}$ and the $T-H^b$ planes and suggested the possible spin configurations before and after the transitions. Furthermore, we analyzed the experimental data in the framework of the molecule field theory and discussed the origin of the spin-canting, the metamagnetism, and the spin-flop transition. The intrinsic parameters of this magnetic system, such as the intra- and interlayer interactions (J and J^{a*}), the exchange field (H_E), the anisotropy field (H_A), and the anisotropy parameter (α) were deduced successfully. The rather small α and the ratio J^{a*}/J ensure that **1** is a two-dimensional Heisenberg magnetic system.

Experimental Section

General Remarks. All starting materials were commercially available, reagent grade, and used as purchased without further purification. The ligand btr was prepared according to the literature method.[19] Elemental analysis of carbon, hydrogen, and nitrogen was carried out with an Elementary Vario EL. The micro-infrared spectroscopy studies were performed on a Magna-IR 750 spectrophotometer in the 4000−500 cm^{-1} region. Variable-temperature magnetic susceptibility, zero-field ac magnetic susceptibility measurements, and field dependence of magnetization on a polycrystalline sample and a carefully oriented single crystal were performed on an Oxford Maglab 2000 System or a Quantum Design MPMS XL-5 SQUID system equipped with a horizontal rotator sample holder. All experimental magnetic data except for the rotation data were corrected for the diamagnetism of the sample holders and of the constituent atoms (Pascal's tables).

Synthesis A 5 mL of water solution containing $MnCl_2·4H_2O$ (0.3 mmol) and NaN_3 (0.6 mmol) was added to 5 mL of DMF (DMF = *N*,*N*-dimethylformamide) solution containing 0.3 mmol of btr and stirred for about 20 min. Some precipitates were removed by filtration. Slow evaporation of the filtrated solution at room temperature gave well-shaped hexagonal large (up to $4.0 \times 2 \times 0.5$ mm^3) single crystals of **1** in 2 weeks, yield 60%. Anal. (%). Calcd for $C_8H_8N_{18}Mn$ (411.26): C, 23.27; N, 61.31; H, 1.96. Found: C, 23.52; N, 61.87; H, 2.10. IR (micro-spectrum): 3430w, 3123m, 2089s, 1525w, 1501w, 1296w, 1086m, 1072w, 1005m, 960w, 860m.

Caution: Although it is not encountered in our experiments, azide salts are potentially explosive. Only a small amount of the materials should be prepared, and it should be handled with care.

Single-Crystal X-ray Crystallography. The diffraction intensity data collection for **1** and the identification of the lattice axes orientation with respect to the morphology of the single crystal were performed on a NONIUS Kappa-CCD with Mo Kα radiation ($\lambda = 0.71073$ Å) at 293 K. The structure was solved by the direct method and refined by a full matrix least squares technique based on F^2 using the SHELXL 97 program. The hydrogen atoms of btr were added to calculated positions. The crystal has long plate shape with the *bc* plane within the plate, the *b* axis along the long axis of the sample, and *a** perpendicular to the plate (Figure 1a). The crystallographic data of **1** are listed in Table 1 (CCDC-277083− This can be obtained free of charge at www.ccdc.cam.ac.uk/conts/retrieving.html [or from the Cambridge Crystallographic Data Centre, 12, Union Road, Cambridge CB2 1EZ, UK; fax: +44−1223/336−033; e-mail, deposit@ccdc.cam.ac.uk]). Also, the CIF file of **1** can be found in the Supporting Information.

Results and Discussion

Crystal Structure. Single-crystal X-ray diffraction reveals that **1** crystallizes in the monoclinic space group $P2_1/c$, and the layer structure (Figure 1) is quite similar to those reported compounds with (4,4) layers constructed by metal ions and EE azido linkers.[7b,14] Each Mn^{2+} ion is located in the inversion center (Figure 1b) and octahedrally coordinated by four bridging EE N_3^- within the layer and two terminal btr ligands above and below the layer via one of their N atoms in the triazole ring. The MnN_6 octahedron is slightly compressed with four long Mn−N bonds of Mn1−N1 = Mn1−N1C = 2.243 Å, Mn1−N7 = Mn1−N7C = 2.233 Å and two short ones of Mn1−N9A = Mn1−N9B = 2.200 Å in which the N atoms belong to one pair of azido. The cis N−Mn−N angles range between 87.75 and 92.25° while the trans ones are of ideal 180°. The neutral 2D (4,4) layer lies in the *bc* plane, with the *b* and *c* axes crossing two diagonal lines of the grids (Figure 1c) with edges of 6.023×6.023 Å, which are the intralayer Mn···Mn distances spanned by EE azido ions. There are two structural features that are related to the magnetic properties of **1** being discussed in detail later. (i) The EE azido bridges can, as having been well demonstrated, efficiently intermediate AF coupling between the Mn^{2+} ions.[7b,14] (ii) Because of the lack of inversion center halfway of the adjacent spins and the axes of adjacent MnN_6 octahedra are tilted with each other (the torsion angle $N_{btr}-Mn-Mn-N_{btr}$ is 74.60°), the weak-ferromagnetism due to spin-canting, originated from the antisymmetric interaction and the existence of an anisotropy, is allowed.[4,20,21] Several reported compounds with 2D (4,4) layer of Mn^{2+} and EE azide do behave as weak-ferromagnets.[7b,14a−d]

Between the layers, weak hydrogen bonds were found between N6 of btr in one layer and C1−H1 of btr in the adjacent layer (Figure 1d). The H-bond geometries are the

---

(16) (a) De Munno, G.; Julve, M.; Viau, G.; Lloret, F.; Faus, J.; Viterbo, D. *Angew. Chem., Int. Ed. Engl.* **1996**, *35*, 1807−1810. (b) Cortés, R.; Lezama, L.; Pizarro, J. L.; Arriortua, M. I.; Fojo, T. *Angew. Chem., Int. Ed. Engl.* **1996**, *35*, 1810−1812. (c) De Munno, G.; Poerio, T.; Viau, G.; Julve, M.; Lloret, F.; Journaux, Y.; Rivière, E. *Chem. Commun.* **1996**, 2587−2588.

(17) (a) Han, S.; Manson, J. L.; Kim, J.; Miller, J. S. *Inorg. Chem.* **2000**, *39*, 4182−4185. (b) Martín, S.; Barandika, M. G.; Lezama, L.; Pizarro, J. L.; Serna, Z. E.; De Larramendi, J. I. R.; Arriortua, M. I.; Rojo, T.; Cortés, R. *Inorg. Chem.* **2001**, *40*, 4109−4115. (c) Fu, A. H.; Huang, X. Y.; Li, J.; Yuen, T.; Lin, C. L. *Chem. Eur. J.* **2002**, *8*, 2239−2247.

(18) (a) Manson, J. L.; Arif, A. M.; Miller, J. S. *Chem. Commun.* **1999**, 1479−1480. (b) Hao, X.; Wei. Y. G.; Zhang, S. W. *Chem. Commun.* **2000**, 2271−2272.

(19) Haasnoot, J. G.; Groeneveld, W. L. Z. *Naturforsch.* **1979**, *34b*, 1500−1506.

(20) (a) Moriya, T. *Phys. Rev.* **1960**, *120*, 91−98. (b) Moriya, T. *Phys. Rev.* **1960**, *117*, 635−647.

(21) Dzialoshinski, I. *J. Phys. Chem. Solids* **1958**, *4*, 241−255.

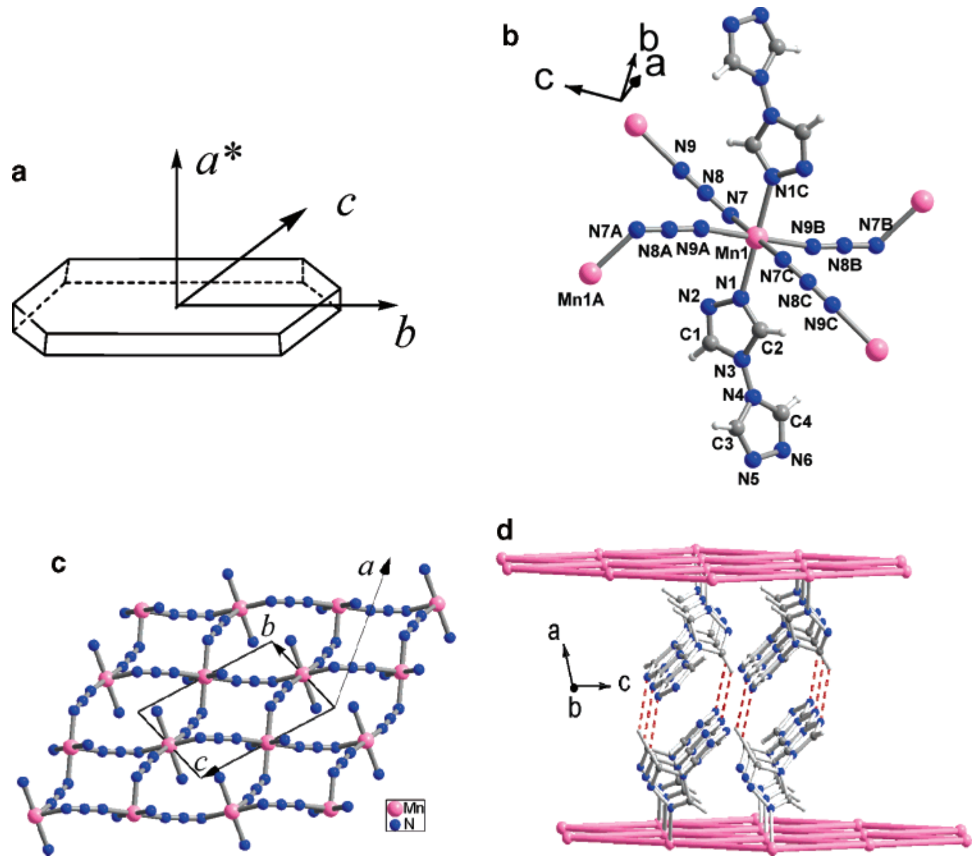

Figure 1. (a) Morphology of the single crystal of **1**. (b) Local environment of Mn with atoms labeled. (c) The (4,4) network in *bc* plane bridged by *EE* azide. btr is omitted for clarity. (d) 3D structure of **1** with weak C−H···N bonds. Only several btr are depicted for clarity.

Table 1. Crystallographic Data for Compound 1

formula	$C_8H_8N_{18}Mn$	crystal size [mm^{-1}]	0.18 × 0.25 × 0.40
M_r [gmol^{-1}]	411.26	μ(Mo Kα) [mm^{-1}]	0.899
crystal system	monoclinic	measured refl.	12944
space group	$P2_1/c$	independent refl.	1773
a [Å]	12.2831(4)	observed refl.[a]	1363
b [Å]	6.3680 (1)	no. of parameters	125
c [Å]	10.2245(3)	GOF	1.026
β [°]	105.064 (1)	max/min (e·Å^{-3})	0.209/−0.199
V [Å^3]	772.27 (4)	T_{max}/T_{min}	0.854/0.810
Z	2	$R1$[b]	0.0262
ρ_{calcd} [g·cm^{-3}]	1.769	$wR2$[c]	0.0687

[a] Observation criterion: $I \geq 2\sigma(I)$. [b] $R1 = \Sigma||F_o| - |F_c||/\Sigma|F_o|$, for observations [c] $wR2 = \{\Sigma[w(F_o^2 - F_c^2)^2]/\Sigma[w(F_o^2)^2]\}^{1/2}$, for all data.

distances of N6···H1 and N6···C1 being 2.62 and 3.19 Å, respectively, and the C−H···N angle of 120°. Each btr of one layer thus forms two C−H···N hydrogen bonds with two btr ligands in the adjacent layer, giving the corresponding interlayer Mn···Mn distances of 12.430 Å. Thus, from the viewpoint of magnetism, the interlayer magnetic interaction is expected to be very weak compared to the intralayer interaction, giving a good example of a local $S = 5/2$ 2D Heisenberg magnetic system. However, at low temperatures, the weak interlayer exchange interaction, mediated by either dipole−dipole interaction or *H*-bonds,[23] does play an important role in tuning the complicated magnetic behavior of **1**.

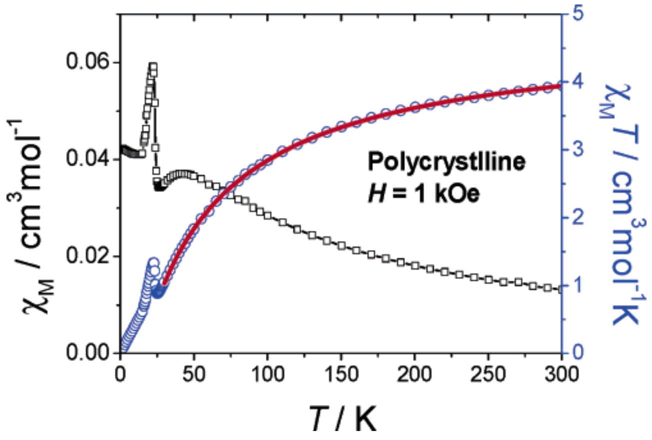

Figure 2. Temperature dependences of χ_M and $\chi_M T$ for a polycrystalline sample. The line across $\chi_M T$ curve represents the best fit by Line's mode.

Magnetic Properties: dc and ac Susceptibility of a Polycrystalline Sample. The temperature-dependent susceptibility of a polycrystalline sample in 2−300 K under an applied field of 1 kOe is shown in Figure 2 ($\chi_M T(T)$ and $\chi_M(T)$). After reaching a broad maximum ($\chi_{max} = 0.037$ cm^3 mol^{-1}) at ca. 42 K, the χ_M decreases slightly with decreasing temperature till 24 K, then increases abruptly to a peak at about 22 K, and decreases again slowly to a constant value of 0.041 cm^3 mol^{-1} below 15 K. The sharp peak indicates the occurrence of a long-range ordering state below 24 K, which may be caused by the spin-canting. The $\chi_M T$ value decreases gradually from the room temperature value of 3.95 cm^3 mol^{-1} K, lower than the spin-only value 4.375 cm^3 mol^{-1} K for Mn^{2+} of $S = 5/2$, to a minimum at 25 K, and then increases to a peak at 22.5 K with a further decrease till 2 K. Fitting of the data above 100 K with the Curie−Weiss law gives $C = 4.77$ cm^3 mol^{-1} K and a negative $\theta = -60.8$ K, indicating a strong intralayer AF coupling.

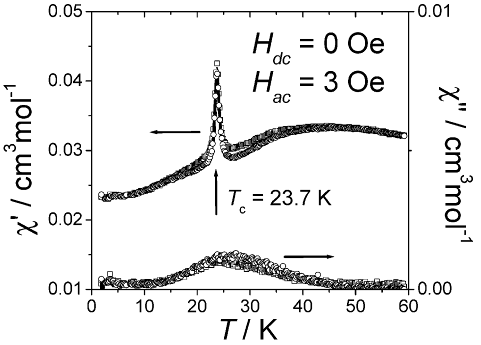

Figure 3. Temperature dependences of the ac susceptibility for a polycrystalline sample.

To evaluate the intralayer magnetic coupling constant J between the Mn^{2+} ions, the theoretical estimates for the Heisenberg lattice with $S = 5/2$ in a (4, 4) layer were given by de Jough and Miedema[24] as the following equations with the Hamiltonian $H = -\sum_{\langle i,j\rangle} JS_i\cdot S_j$:

$$kT(\chi_{\max})/\left|\frac{J}{2}\right|S(S+1) = 2.05 \tag{1}$$

$$\chi_{\max}\left|\frac{J}{2}\right|/Ng^2\beta^2 = 0.0551 \tag{2}$$

In eqs 1 and 2, k, N, g, and β have their usual meanings. $\chi_{\max}$ and $T(\chi_{\max})$ are the observed susceptibility maximum and the temperature of the maximum, saying $\chi_{\max} = 0.037$ cm^3 mol^{-1} and $T(\chi_{\max}) = 42$ K. We obtain $J = -3.26$ cm^{-1} and -3.10 cm^{-1} (taking $g = 2.00$), respectively. Furthermore, the high-temperature susceptibility data were also fitted to the high-temperature series expansion of Lines[25] for an $S = 5/2$ *AF* (4,4) layer using

$$\chi T = \frac{Ng^2\beta^2 T}{J}\left(3x + \sum_{n=1}^{6}\frac{C_n}{x^{n-1}}\right)^{-1} \tag{3}$$

with $x = k_BT/JS(S + 1)$, $C_1 = 4$, $C_2 = 1.448$, $C_3 = 0.228$, $C_4 = 0.262$, $C_5 = 0.119$, and $C_6 = 0.017$. The best fitting gives $J = -3.35(1)$ cm^{-1} and $g = 2.024(1)$, with $R = 6.7 \times 10^{-5}$ $[R = [\sum((\chi T)_{obs} - (\chi T)_{calc})^2/\sum((\chi T)_{obs})^2]$. All of these J values obtained above are in agreement with each other and are comparable with those related Mn^{2+} compounds.[14]

The temperature dependences of the in-phase (χ'_M) and the out-of-phase (χ''_M) ac magnetic susceptibilities under $H_{dc} = 0$ Oe and $H_{ac} = 3$ Oe with frequencies 666 and 1633 Hz were measured from 2 to 60 K, as depicted in Figure 3. The χ'_M exhibits a broad maximum around 40 K and a sharp peak at $T_N = 23.7$ K; and χ''_M also shows a broad peak between 20 and 30 K, again indicating the onset of long-range ordering state.

Magnetic Study upon Single Crystal of 1. The measurements were performed on a single crystal of 1.56 mg with the lattice axes orientation and the morphology sketched in Figure 1a. The orientation accuracy of axes were estimated several degrees during the measurements.

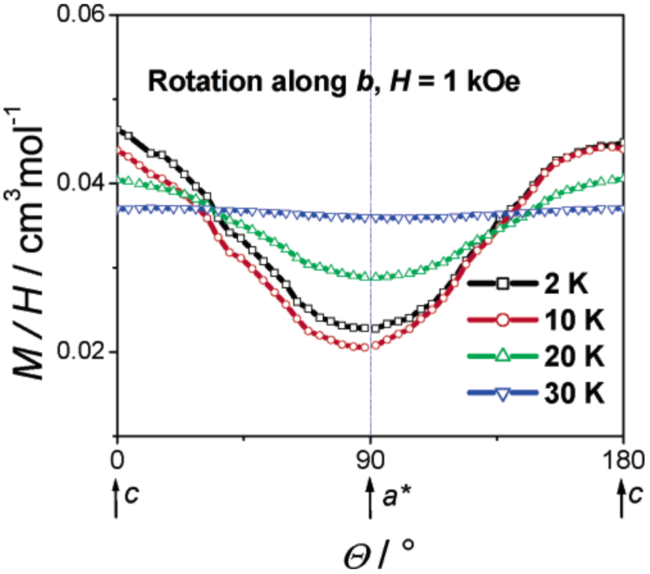

Figure 4. Angular dependences of magnetization under 1 kOe in the a^*c plane at different temperatures ($\Theta = 0°$, H // c).

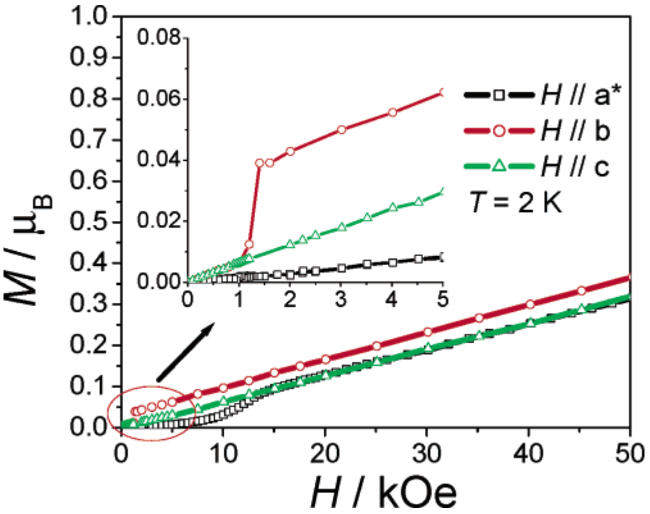

Figure 5. Field dependences of the magnetization at 2 K along the a^*, b, and c axes.

Determination of the Magnetic Axes. Since the space group of **1** is $P2_1/c$, the 2-fold axis of the monoclinic lattice (b) is necessarily one of the magnetic axes. The other two axes may be determined from the extremes of the magnetization in the *ac* plane. As can be seen from the results measured in 1 kOe at 2, 10, 20, and 30 K (Figure 4), these extremes were found to be along the a^* ($\Theta = 90°$) and c ($\Theta = 0°$) directions. Thus, the crystallographic axes a^*, b, and c are the magnetic axes. It should be noted here, that the a^* axis is perpendicular to the manganese azide layers as they are parallel to the *bc* plane. Hereafter we use the symbol A^B to represent the magnetic parameter A along the direction B (a^*, b, or c).

Field Dependences of the dc Magnetization. The field dependences of the magnetization $M(H)$ measured with increasing the fields up to 50 kOe at 2 K along the a^*, b, and c axes were displayed in Figure 5. Along b, the M^b increases slowly from zero to ca. 0.006 μ_B at 1 kOe, after a

---

(22) Silvera, I. F.; Thornley, J. H. M.; Tinkham, M. *Phy. Rev.* **1964**, *136*, A695−A710.

(23) Harrison, A.; Clarke, S. J.; Mason, T. E.; Visser, D. *J. Magn. Magn. Mater.* **1992**, *104*−107, 557−558.

(24) De Jough, L. J.; Miedema, A. R. *Adv. Phys.* **1974**, *23*, 1−260.

(25) Lines, M. E. *J. Phys. Chem. Solids* **1970**, *31*, 101−106.

jump up to 0.039 μ_B at 1.4 kOe, it increases linearly to 0.366 μ_B till 50 kOe, which is far from the expected saturation value $M_S = 5.0\ \mu_B$ for one Mn^{2+} ion. The extrapolation to zero field of the data in high fields has a positive intercept (0.031 μ_B) to the M axis, indicating a WF behavior. No hysteresis loop around $H = 0$ Oe was observed. The M^c curve below 1 kOe is coincident with M^b, however, it increases to 0.321 μ_B in 50 kOe showing no deviation from the linearity. As for M^{a*}, it increases more slowly than M^b and M^c do till about 8 kOe, and then after increasing gradually with the field until 14 kOe, it goes coincidentally with M^c. Different from M^b, the extrapolation of M^{a*} in the high fields goes straightly across the origin, suggesting no net moment is generated during the phase transition.

This kind of field-dependent behavior is quite interesting. First, the maximum (0.366 μ_B) of the magnetization at 50 kOe is only about 8% of M_S, indicating the strong AF couplings between the Mn^{2+} ions. Second, the magnetization behaviors along three axes are different from each other. In the low field region ($H < 1$ kOe), M^b and M^c seem to be identical and larger than M^{a*}. It is evidenced for an antiferromagnet with spins parallel to the a^* axis. When the applied fields are in the middle region (1 kOe $< H <$ 14 kOe), M^b departs from M^c through a sudden jump. The further increase of the fields ($H >$ 14 kOe) results in another spin state: M^b remains the largest, while M^{a*} and M^c are now almost equal. From the maximums of the dM/dH curves, the critical fields (H_c) for the transitions at 2 K with fields along b and a^* are determined to be H_c^b (2 K) = 1.2 kOe and H_c^{a*}(2 K) = 12.5 kOe, respectively. As will be discussed in detail later, the transition along b reflects a metamagnetic transition from an AF state in the form of a hidden spin-canting to a WF state due to the emergent spin-canting. The transition with field along a^* is likely a spin-flop one with an external field parallel to the spin alignment for an antiferromagnet.[4,11]

To obtain more information of the magnetic phase transitions, the field dependences of $M^b(H)$ and $M^{a*}(H)$ at different temperatures were investigated carefully upon both sweeping up and down of the applied field. As shown in Figure 6a, all the M^b curves below 24 K have similar characters as that at 2 K, showing an abrupt transition at the critical field H_c^b. The H_c^b and the magnetization above 1.2 kOe decrease with increasing temperature from 2 to 22 K. At 30 K ($> T_N$), M^b increases linearly without any transition, showing a paramagnetic behavior. Most interestingly, we observed a hysteresis behavior of M^b when H_c^b was approached from the fields below or above H_c^b. Consequently, we can get two different H_c^b values, $(H_c^b)_{up}$ and $(H_c^b)_{down}$, at each temperature. The width of the loop defined by $\Delta H_c^b = (H_c^b)_{up} - (H_c^b)_{down}$ at 2 K is $\Delta H_c^b = 50$ Oe. These data (T, H_c^b) determine part of the phase boundaries in the $T-H^b$ plane, and these two H_c^a values give a narrow critical region with two phases mixed (Figure 10, vide post).

Along a^* (Figure 6b), the situation is somewhat similar to that along b: the higher the temperatures, the less pronounced the transitions; and the transition disappears above T_N. Different from M^b, no hysteresis loops were observed in M^{a*}. Besides, we can estimate the critical fields (H_c^{a*}) as mentioned before and determine part of the phase boundaries in the magnetic phase diagram in the $T-H_c^{a*}$ plane.

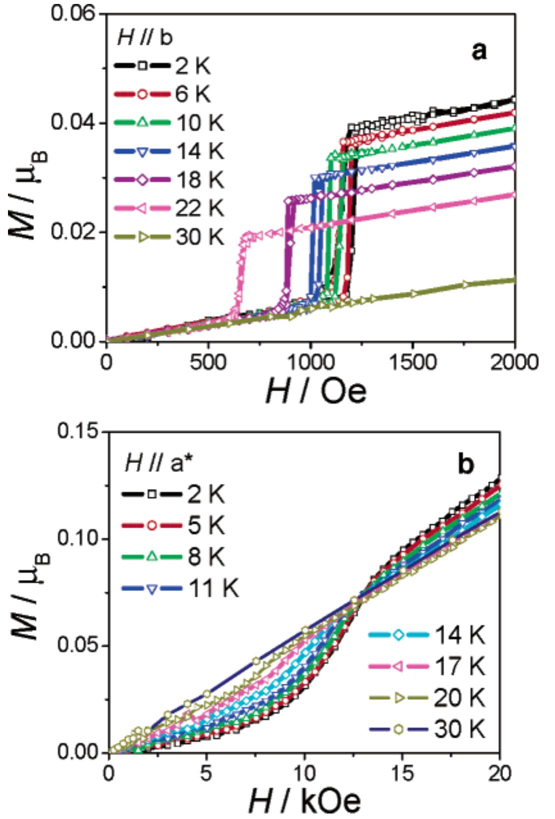

Figure 6. Field dependences of the magnetization along the b and a^* axes at different temperatures.

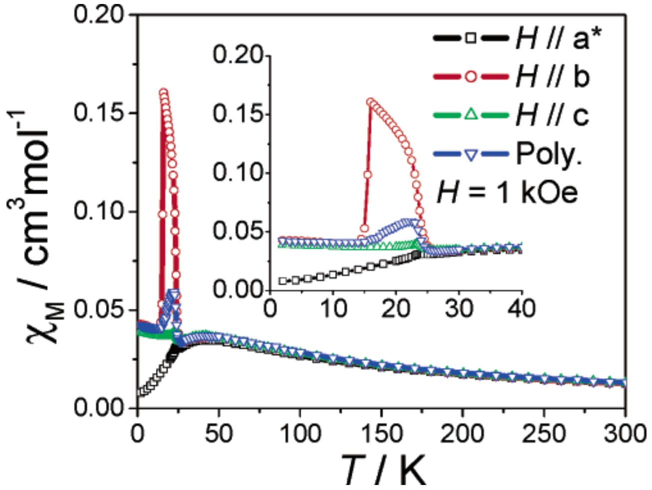

Figure 7. Temperature dependences of the susceptibilities along the a^*, b, and c axes together with that for a polycrystalline sample.

Temperature Dependences of the dc Magnetic Susceptibility and Magnetization. The temperature dependences of the susceptibility χ_M from 2 to 300 K under 1 kOe along three magnetic axes are displayed in Figure 7, together with the result for the polycrystalline sample. At high temperatures (>40 K), the curves all show broad peaks at about 40 K and almost superpose together, reflecting the AF coupling and the isotropic behavior of the ^6A ground state of Mn^{2+}. Upon temperature going down from 30 K, χ_M values are anisotropic. χ_M^{a*} shows a small peak at 23.7 K and then decreases further toward zero at 2 K. χ_M^c has a more

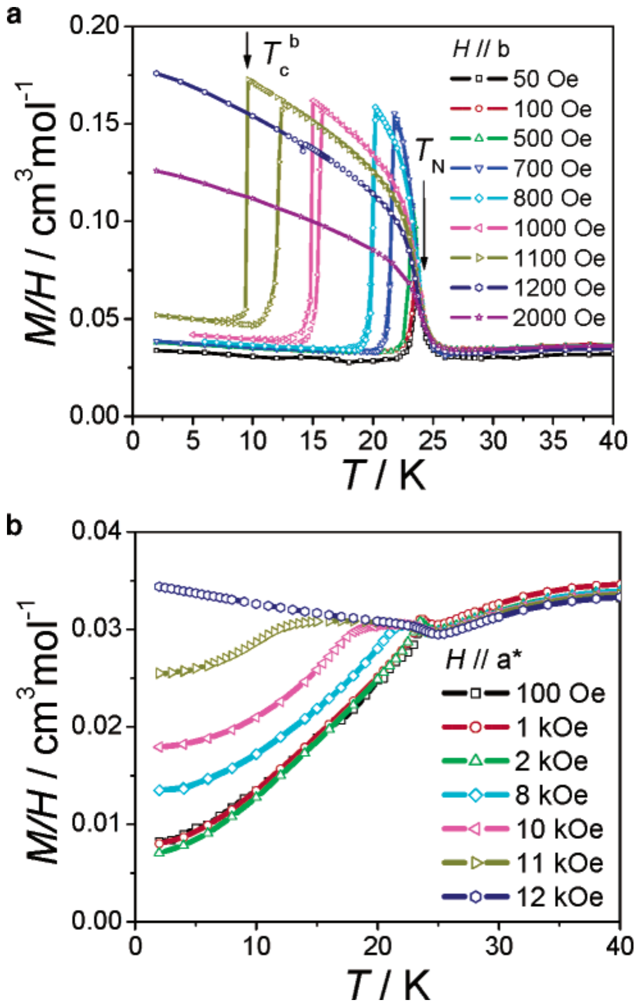

Figure 8. Temperature dependences of magnetization under different fields: (a) *H* // *b* and (b) *H* // *a**.

pronounced peak at 23.7 K, and then after a small decrease, it remains almost constant till 2 K. $\chi_M{}^b$ displays a more complex behavior with two magnetic phase transitions. On cooling $\chi_M{}^b$ first increases abruptly from 0.038 cm^3 mol^{-1} (25 K) to 0.160 cm^3 mol^{-1} (16 K), and then it decreases rapidly to 0.044 cm^3 mol^{-1} at 14.5 K and keeps almost constant till 2 K. Below 14.5 K, $\chi_M{}^b$ and $\chi_M{}^c$ are almost equal, and higher than $\chi_M{}^{a*}$. This behavior is consistent with an AF ordered system. $\chi_M{}^{a*}$ represents the parallel susceptibility $\chi_{//}$, and both $\chi_M{}^b$ and $\chi_M{}^c$ are the perpendicular ones $\chi_\perp$. This observation is consistent with the results from *M*(*H*) at 2 K and confirms that the *a** axis is the easy-axis in the AF state. However from 14 to 24 K, the observed spontaneous magnetization is stronger along the *b* axis, intermediate along the *c* axis, and not present along the *a** axis. This implies that a WF state is formed along the *b* axis. Incorporating the metamagnetic behavior along *b* discussed above, we may attribute these phenomena to a hidden spin-canting with four antiferromagnetic sublattices. Under 1 kOe, the AF region with the hidden spin-canting falls in the temperature region 2−14 K, and the WF region with the net moment along *b* is in the region of 14 to 24 K.

Furthermore, the magnetization $M^b(T)$ and $M^{a*}(T)$ at different fields in comparison to *M*(*H*) results were investigated in temperature region of 40 K to 2 K when the external fields were in 50−2000 Oe along *b* and 100−12000 Oe along *a**. The magnetization was measured in both cooling and warming procedures. $M^c(T)$ was not checked in this batch because the linear $M^c(H)$ (Figure 5) provided less information we presumed. The measurement results are presented in Figure 8.

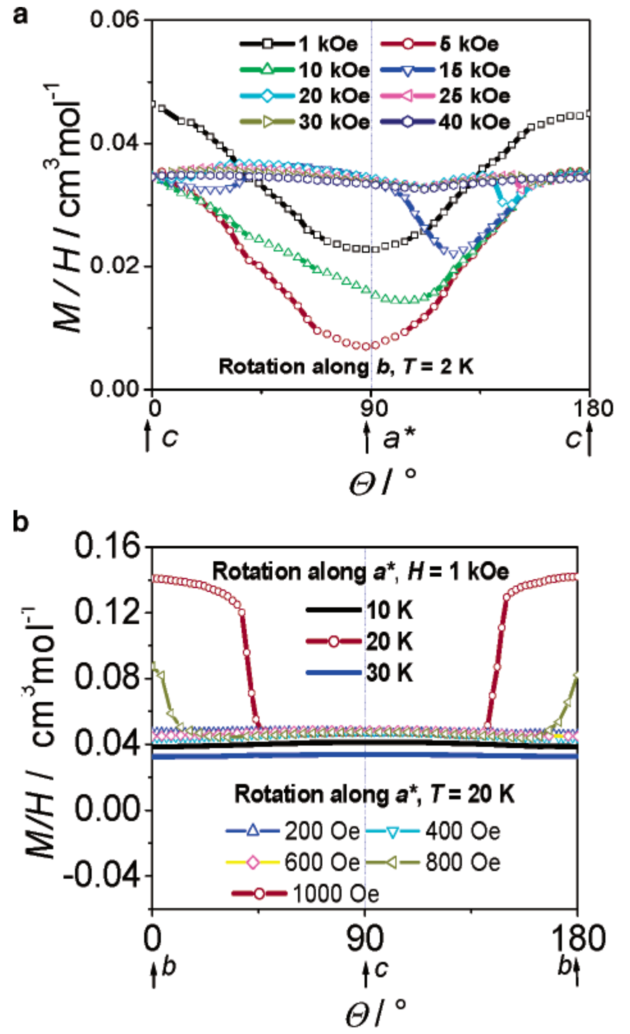

Figure 9. (a) Angular dependences of the magnetization in *a***c* plane at 2 K under different external fields (Θ = 0°, *H* // *c*). (b) Angular dependences of the magnetization in *bc* plane: under 1 kOe at 10, 20, and 30 K and at 20 K under different external fields (Θ = 0°, *H* // *b*).

As shown in Figure 8a, in low external fields (50, 100 Oe), $M^b(T)$ shows a peak at ca. 24 K. The WF region is very narrow, and the state below 24 K is mostly the AF state. The field-cooled and zero-field-cooled magnetization reveals no significant difference. Although the small signal of our small single-crystal sample prevents us from measuring the magnetization using very low field, it seems that the WF region will disappear when the external field becomes zero. When the applied field is stronger, the WF region becomes wider. For the external fields we used, the width of the WF region reaches the maximum when $H = 1.1$ kOe. The further increase of the field (≥1200 Oe) removes totally the AF state above 2 K, and only the WF state is kept. The critical temperature ($T_c{}^b$) for the AF to WF transition and the Néel temperature ($T_N{}^b$) are deduced from the positive and negative peaks on d*M*/d*T*, respectively. Since the transition from the paramagnetic state to the magnetically ordered state is hardly influenced by the external field, the Néel temperature ($T_N{}^b$)

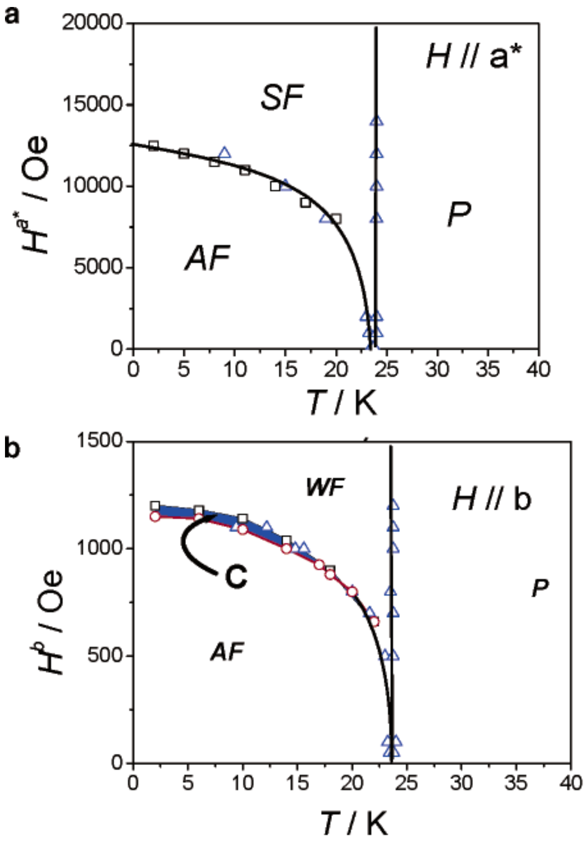

Figure 10. Magnetic phase diagrams: (a) *H* // *a** and (b) *H* // *b*. The squares and dots are from the *M*(*H*) curves and the triangles are from the *M*(*T*) curves. The blue region in ($T-H^b$) is the critical domains where the hysteresis loops can be observed. The full lines are just to guide the eye.

changes little with the external field. However, $T_c^{\,b}$ strongly depends on the external field: the higher the field, the lower the $T_c^{\,b}$. These points ($T_c^{\,b}$, H) and ($T_N^{\,b}$, H), together with those (T, $H_c^{\,b}$) data from the isothermal $M^b(H)$ measurements, complete the boundaries of the magnetic phase diagram in the $T-H^b$ plane.

Similar to the loops in $M^b(H)$ curves, an obvious hysteresis effect, which is clearly seen from the curve measured under 800 Oe, and more obviously in those under 1.0 and 1.1 kOe, can also be observed in $M^b(T)$. Defined by $\Delta T_c^{\,b} = (T_c^{\,b})_{up} - (T_c^{\,b})_{down}$, the widths of the loops in 1.0 and 1.1 kOe are $\Delta T_c^{\,b} = 0.8$ and 3.8 K, respectively. The existence of this kind of loops indicates that the phase transition occurs at different temperatures depending on whether the transition region is approached from the high- or low-temperature side. According to Levinson,[26] the phase transition from AF to WF state is of first order.

Along the *a** direction (Figure 8b), $M^{a^*}(T)$ shows a peak near 24 K and decreases smoothly further in lower fields (H = 100, 1000, and 2000 Oe). The higher field stretches the peaks to a broad platform, and the higher the field, the wider the platform. Fields higher than 12 kOe totally remove the AF state, and thus $M^{a^*}(T)$ increases monotonically from 24 to 2 K. No hysteresis effect was observed along *a**. Also from the curves of dM/dT, $T_c^{\,a^*}$, and $T_N^{\,a^*}$ can be obtained. The field dependences of $T_N^{\,a^*}$ and $T_c^{\,a^*}$ are quite similar to those along *b*. These data ($T_c^{\,a^*}$, H) and ($T_N^{\,a^*}$, H) give the boundaries of the phase diagram in the $T-H^{a^*}$ plane, as in the $T-H^b$ plane.

Angular Dependences of the Magnetization in the *a*c* and *bc* Planes. The metamagnetic transition from the AF to WF state and the spin-flop transition should be associated with the change of the spin axes. To further characterize them in detail, the angular dependences of the magnetization in the *a*c* and *bc* planes were investigated under several external fields at different temperatures.

As discussed above, the *a** axis is the easy-axis in the AF state, and the anisotropy in the *a*c* plane is reduced significantly when the external field increases up to 14 kOe (see Figure 5). To further prove this, angular dependences in the *a*c* plane at 2 K under several fields from 1 kOe to 40 kOe were measured and depicted in Figure 9a. It is clear that under lower fields, say 1 and 5 kOe, the extremes are found with $\Theta = 0°$ and 90° and the easy-axis is still along the *a** axis. When the external field is very high ($H \geq 20$ kOe), the difference between the magnetization along *a** and *c* is reduced and the *a*c* plane becomes almost isotropic. Now the extremes of magnetization are no longer along $\Theta = 0°$ or 90°, reflecting the departure of magnetic axes from the *a** and *c* axes. When the field is 10 kOe, the maximum remains along the *c* direction ($\Theta = 0°$) and the minimum moves to another direction ($\Theta = 104°$). When the field is larger than 10 kOe, an even more complicated behavior was observed. For example, there are four local extremes observed when $H = 15$ kOe ($\Theta = 28°$ and 124° for the minimum, and $\Theta = 0°$ and 60° for the maximum). The exact reason for the change of the extremes is not clear now, but we think it might originate from the spin configuration in the SF state and the domain structure of **1**.

In the *bc* plane, the angular dependences of the magnetization confirm the metamagnetic transition. First, the magnetization was measured under 1 kOe at 10, 20, and 30 K (Figure 9b). At 10 K, the magnetization is maximum along *c* ($\Theta = 90°$) and minimum along *b* ($\Theta = 0°$). At 20 K, a significant change happens. The maximum now changes to *b* ($\Theta = 0°$) and the minimum along a wide range of direction ($50° < \Theta < 140°$). A further increase of the temperature up to 30 K in the paramagnetic region changes the situation back. The difference between the magnetization along *b* and *c* axes at 10 and 30 K is actually very small (about 7% and 4% of the magnetization). It means that in the AF and paramagnetic states, the *bc* plane is almost isotropic. Furthermore, we measured the angular dependences of magnetization in the *bc* plane at 20 K under different external fields (see also Figure 9b). Under low fields (<600 Oe), the *bc* plane remains isotropic and the magnetization along *c* ($\Theta = 90°$) is slightly larger than that along *b*. When the field increases to 800 Oe, a strong anisotropy is induced by the field. The magnetization is maximum along *b* ($\Theta = 0°$) and decreases quickly to the minimum in the $12° < \Theta < 168°$ region. A further enhanced field to 1 kOe widens the region of the easy-magnetization.

Now several fundamental aspects are confirmed clearly. First, the easy-axis in the AF state is along *a**. This is consistent with the $\chi_{//}$ and $\chi_{\perp}$ for a normal antiferromagnet

---

[26] Levinson, L. M.; Luban, M.; Shtrikman, S. *Phys. Rev.* **1969**, *187*, 715−722.

below the Néel temperature. Second, in the WF state, *b* is the easy-magnetization direction, which means that the net weak ferromagnetic moment is along *b*. Third, an increase of the field (e.g., at 20 K, the field up to 800 Oe, Figure 9b) will lead to the metamagnetic transition to the WF state from a hidden spin-canting state. Because of the same energetic effect of the field and the temperature, an increase of the temperature under a constant field will cause the transition too (e.g., from 10 to 20 K under 1 kOe, Figure 9b). Consequently, all the experimental results can be understood in the frame of hidden spin-canting, metamagnetism, and spin-flop states.

It is now convenient to briefly compare the fundamental aspects of **1** with the well-known phenomenon named Morin transition.[21,27] This transition at T_M is specific to α-Fe_2O_3, characterized by a change in magnetic structure from a WF state at high temperatures, with the spins lying in the basal plane (111) and slightly canted, to a pure AF state at low temperatures, with the spins parallel to the [111] direction. The similar transition has also been observed in ϵ-Fe_2O_3 and CuB_2O_4.[28,29] Although the main properties, including the spin-canting, the spin-flop, and the field dependent behavior, of **1** and α-Fe_2O_3 are similar, they are distinguished from each other in the following. (i) The canting is intrinsic for **1**, and the ground state is an AF state with hidden spin-canting. While for α-Fe_2O_3, the canting can exist only at $T > T_M$, and the ground state at low temperatures is a pure AF state. (ii) The spin-flop of **1** can only be induced by external fields parallel to *a**, while in α-Fe_2O_3 it can be induced either by temperature or external fields, which was confirmed by the zero-field neutron diffraction and Mössbauer spectrum studies.[27b−c]

Magnetic Phase Diagram. Let us summarize the obtained magnetic feature of this material. The magnetic interaction between adjacent Mn^{2+} ions through the EE azide is clearly antiferromagnetic, and the interlayer coupling should also be weak antiferromagnetic. The magnetic axes were found to be the *a**, *b*, and *c* crystallographic axes. The AF, WF, SF, and paramagnetic state were observed in this unique system under certain conditions. The phase transition from paramagnetic state to a long-range ordered state occurs at $T_N = 23.7$ K regardless of the external field. Below T_N, the lower temperature and field stabilize the AF state, while the higher temperature and field stabilize the WF or SF state. From the systematic measurements on $M(T)$ and $M(H)$ along *a** and *b*, we obtained a series of (T, H^{a*}) and (T, H^b) critical values, which produces the magnetic phase diagrams in the $T-H^{a*}$ and $T-H^b$ planes (Figure 10).

In the $T-H^{a*}$ plane (Figure 10a), there are three regions: **AF**, **SF**, and **P**, respectively. The region **AF** corresponds to the hidden spin-canting phase. With fields along *a**, an increase of temperature or field will cause the phase transition to the **SF** phase. The region **P** represents the paramagnetic phase at high temperatures and normal fields. Similar, but a little bit complex, phase diagram is obtained in the $T-H^b$ plane. Now, the region **WF** corresponds to the weak-ferromagnetic state where the hiding of spin-canting is broken. The transition between **AF** and **WF** states should be of first-order because of the observation of different hysteresis effect in $M^b(H)$ and $M^b(T)$ curves.[26] Interestingly, the hysteresis effect leads to a narrow critical region **C** in the $T-H^b$ plane. As the system passes through this region from one side to the other, a phase transition achieves only when the system leaves this region. Thus, we can conveniently estimate the width ($\Delta H_c{}^b$ and $\Delta T_c{}^b$) of the hysteresis loops in $M^b(H)$ and $M^b(T)$ curves under a certain condition from this phase diagram.

Because the available maximum field 50 kOe of our SQUID system cannot induce transition from the *SF* or *WF* to *P* state, the regions **SF** and **WF** have only part of the boundary to the phase **P**. However, we can infer that there should be a higher critical field which can enforce these *SF* and *WF* states to the paramagnetic phase, as will be discussed below.

Discussion

Origin of the Spin-Canting and Metamagnetic Transition with *H* // *b*. The spin canting was first realized by Dzyaloshinsky in a phenomenological study of α-Fe_2O_3, and a firm theoretical basis was given by Moriya.[4,20−21] It has been widely investigated for many compounds, and observed for several metal−azido systems. Generally, spin-canting can arise from two different sources. The first one is due to an antisymmetric component of the superexchange interaction (*D*zyaloshinsky−*M*oriya *i*nteraction, DMI). The second one is the existence of an anisotropy causing a different preferential direction for the magnetic moments of ions *i* and *j*, which are located on different sublattices. The structural feature of **1** is allowable for both, but we will demonstrate below that the DMI dominates the spin-canting in **1**.

Considering the DM interaction, the Hamiltonian to describe this magnetic system can be written as

$$H = -\sum J(S_i^b \cdot S_j^b + S_i^c \cdot S_j^c) - \sum J^{a*}(S_i^{a*} \cdot S_j^{a*}) - \sum \vec{\boldsymbol{D}}_{ij} \cdot [\mathrm{S}_i \times \mathrm{S}_j] - g\mu_B \vec{H} \cdot \sum \vec{S}_j \quad (4)$$

The quantity $\boldsymbol{D}_{ij}$ is the DM vector. This coupling acts to cant the spins because the coupling energy is minimized when the two spins are perpendicular to each other. It has been proved that the more anisotropic the system is, the more important the canting will be, for the magnitude of $\boldsymbol{D}_{ij}$ can be estimated to be $|D_{ij}/J| = (g - g_e)/g$. The g value used for this estimation is the one in the direction of $\boldsymbol{D}_{ij}$ and g_e is the free electron g value, $g_e = 2.0023$. From the fitting of the susceptibility along the *b* axis using the Curie−Weiss law, $g_b(\text{canting}) = 2.028$ is obtained. Thus we can estimate that the magnitude of $|\boldsymbol{D}_{ij}/J|$ is about 0.013. As compared to some other values reported (e.g., $(g - g_e)/g \sim 10^{-3}$ for α-Fe_2O_3 and $MnCO_3$),[20] this value is quite large and can lead to an observable spin-canting.

---

(27) For examples, see: (a) Morin, F. J. *Phys. Rev.* **1950**, *78*, 819−820. (b) Worlton, T. G.; Decker, D. L. *Phys. Rev.* **1968**, *171*, 596−599. (c) Simkin, D. J.; Bernheim, R. A. *Phys. Rev.* **1967**, *153*, 621−623. (d) Zysler, R. D.; Fiorani, D.; Testa, A. M.; Suber, L.; Agostinelli, E.; Godinbo, M. *Phys. Rev. B* **2003**, *68*, 212408 and references therein.

(28) Kurmoo, M.; Rehspringer, J. L.; Hutlova, A.; D'Orléans, C.; Vilminot, S.; Estournès, C.; Niznansky, D. *Chem. Mater.* **2005**, *17*, 1106−1114.

(29) Petrakovskii, G.; Velikanov, D.; Vorotinov, A.; Balaev, A.; Sablina, K.; Amato, A.; Roessli, B.; Schefer, J.; Staub, U. *J. Magn. Magn. Mater.* **1999**, *205*, 105−109.

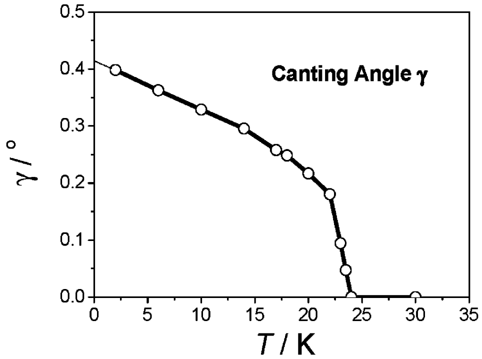

Figure 11. Temperature dependence of the canting angle γ of **1**.

It has been shown that the free energy at $T = 0$ K will be minimal when the canting angle γ is equal to (1/2)arctg(|D_{ij}/J|).[30] Thus, we find the canting angle γ at 0 K to be about 0.37°. Experimentally, we can estimate the canting angle from the $M^b(H)$ measurements (Figure 6a). For the WF state above $H_c{}^b$, the spontaneous magnetization ($M_R{}^b$) is determined by extrapolating the $M^b(H)$ data in the high field region down to zero. The canting angle γ is then related to M_R and M_S through $\sin(\gamma) = M_R/M_S$.[31] With our data, the temperature dependence of the canting angle is obtained (Figure 11). Extrapolating the data to $T = 0$ K, we have $\gamma = 0.42°$, being close to the value 0.37° estimated above. This temperature dependence of γ reveals the increase of the order parameter with decreasing temperature. Similar behavior with a change in the direction of the moments has been observed in $[Mn_3(OH)_2(SO_4)_2(H_2O)_2]$, but it was attributed to the frustration in the Mn_3 trimer in the molecule.[32]

Let us now consider the possible contribution of the local anisotropy to the spin-canting. This mechanism occurs when the local coordination polyhedra of the magnetic ions are tilted with respect to each other.[22] As discussed before, the long axes of the adjacent Mn^{2+} octahedra are tilted. So, symmetrically it may contribute to the spin-canting in **1**. What we need to consider now is the anisotropy energy and its influence on the spin-canting. Two contributions to the total anisotropy energy exist: one arises from the dipolar interaction, the other is due to the single ion anisotropy. Based on our data, we cannot at present calculate them separately. Fortunately, we can reasonably estimate the anisotropy field (H_A) from the spin-flop transition with field along a^* (vide post). The results are $H_A = 0.2$ kOe and $H_E = 387.8$ kOe (H_E is the exchange field defined as $H_E = z|J|S/g\mu_B$).[4,11] The canting angle γ from this mechanism is estimated as follows:[30]

$$\gamma = \frac{\frac{1}{2}H_A \sin 2\theta}{2H_E + H_A \cos\theta} \tag{5}$$

where θ is the angle between the anisotropy field and the a^* axis. For eq 5, the maximum of the canting angle γ is only about 0.00012°, 4 orders smaller than the experimental result. Consequently, the DMI dominates the spin-canting in **1**, similar to another Mn^{2+} compound $(C_3H_7NH_3)_2MnCl_4$.[30]

We now discuss the critical field for the metamagnetic transition in the b direction and the interlayer coupling J^{a*}. Recall that before the transition, the spins in one layer have their net moments along $+b$, whereas those in the adjacent layers are along $-b$. The total energy of all the spins can be deduced from eq 4:

$$E_{\text{total}} = E_0 + NJ^{a^*}S^2 \tag{6}$$

where E_0 represents all the other energy contributions that will not change with H^b. The Zeeman terms $E_Z = -1/2N\mu_B gSH^b \sin\gamma$ due to the adjacent layers cancel each other. After the transition, there is a net moment along b. Now

$$E_{\text{total}} = E_0 - NJ^{a^*}S^2 - N\mu_B gSH^b \sin\gamma \tag{7}$$

The sign of J^{a*} term has changed because the nearest spins in the a^* direction have reversed during the metamagnetic transition.

By equating these two energies, we obtain

$$H_c{}^b = \frac{\frac{1}{2}|J^{a^*}|S}{\mu_B g \sin\gamma} \tag{8}$$

From the phase diagram in the $T-H^b$ plane, we can estimate $H_c{}^b(0\ \text{K}) = 1180$ Oe, and $\gamma(0\ \text{K}) = 0.42°$. The interlayer coupling (J^{a*}) is then calculated to be 6×10^{-4} cm^{-1}, which is 3 or 4 orders smaller than the intralayer exchange coupling (J), reflecting the two-dimensional character of **1**.

Another feature of **1** in the metamagnetic transition is the square hysteretic loops observed in the $M(H)$ curves. It is a manifestation of the first-order phase transition and simply means that the magnetic moment jumps from “up” to “down”. In a thermodynamic sense, the jump from M to $-M$ happens exactly at $H = 0$ since the energies of these two states are equal minimum at this point. Interestingly, the square hysteretic loops in **1** are centered at $H = [(H_c{}^b)_{\text{up}} + (H_c{}^b)_{\text{down}}]/2$, rather than $H = 0$. As discussed above, what happens during the metamagnetic transition is that half of the net moments in the b axis rotate 180° to follow the direction of the field. This is similar to the situation with the loops centered at $H = 0$, except for the influence of the interlayer coupling J^{a*}, which lifts the total energy of the system.

Concerning the origin of spin-canting, we would like to argue the relationship of this phenomenon to the chemical character of the bridging ligands. At the very beginning, canting was observed mostly in some AF materials with spins coupled through a single-atom bridge such as O (Fe_2O_3[27]), Cl ($CsCoCl_3{\cdot}2H_2O$[8a−b]), S (β-MnS[33]), Br ($CoBr_2{\cdot}6D_2O$[34]) etc. Provided that the angle of M−X−M is away from 180°, the single-atom X will always exclude the inversion center

---

(30) Groenendijk, H. A. Differential Suscpetibility Studies of Some Weak Ferromagnets. Ph.D. dissertation, 1981.

(31) Kahn, O. *Molecular Magnetism*; VCH: New York, 1993; p 322.

(32) Salah, M. B.; Vilminot, S.; André, G.; Richard-Plouet, M.; Bourée-Vigneron, F.; Mhiri, T.; Kurmoo, M. *Chem. Eur. J.* **2004**, *10*, 2048−2057.

(33) Keffer, F. *Phys. Rev.* **1962**, *126*, 896−900.

(34) Hijmans, J. P. A.; de Jong, W. J. M.; van den Leeden, P.; Steenland, M. *Physica* **1973**, *69*, 76−86.

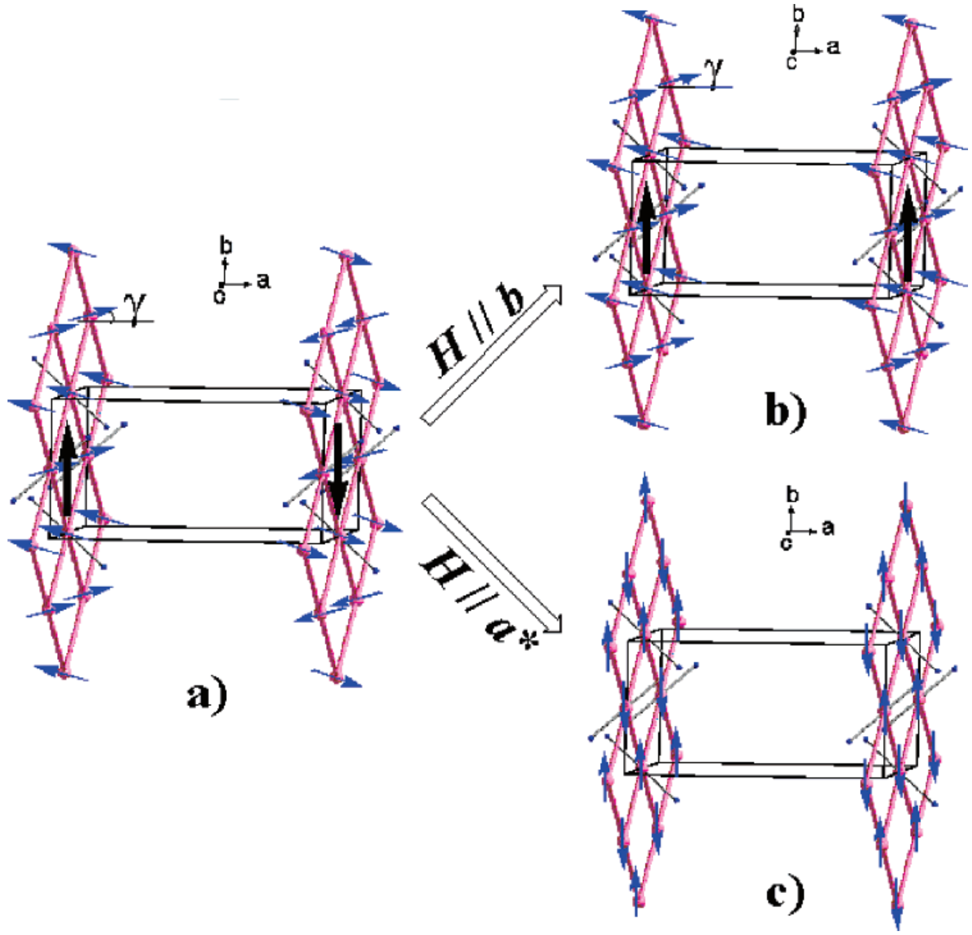

Figure 12. Proposed spin configuration and the phase transitions based on the magnetic data. (a) Hidden spin-canting structure with the easy-axis along *a** and canting along *b*. (b) Weak-ferromagnetic state with net moment along *b* after the metamagnetic transition. (c) Spin-flop state with spins along *b*.

between the bridged two spins and will allow the spin-canting symmetrically. Similarly from the symmetrical point of view, the canting was also frequently observed in AF materials bridged by some three-atom bridges such as N_3^-,[7b,14a−d] $HCOO^-$,[5g−h] and $N(CN)_2^-$(of 1,3 mode)[5b−d] because of the noncentrosymmetrical nature of these bridges. Thus, it might be a reasonable approach to construct the spin-canted molecule-based magnetic materials by considering the bridges with no inversion center.

Spin-Flop Transition with *H* // *a.** Upon application of a field parallel to the preferred axis of sublattice magnetization of an antiferromagnet, a competition is set up between the strength of the external field and the internal exchange field H_E. For an antiferromagnet with weak anisotropy, when H reaches a critical field H_{SF}, the antiparallel magnetizations on the two sublattices flop from the direction of the easy-axis to that perpendicular to it.[4,11] A further increase of the field to H_c' will totally align the spins to the direction of the field, which makes the system to the saturated paramagnetic state. In the molecular field model, the critical fields at $T = 0$ K, $H_{SF}(0)$, and $H_c'(0)$ are related to H_E and H_A by the following equations:[4,11]

$$H_{SF}(0) = (2H_E H_A + H_A^2)^{1/2} \tag{9}$$

$$H_c'(0) = 2H_E - H_A \tag{10}$$

Furthermore, the differential susceptibility dM^{a*}/dH after the SF transition at 0 K can be written as[4,11]

$$dM^{a*}/dH(0) = M_S/(2H_E - H_A) \tag{11}$$

dM^{a*}/dH can be obtained by the differential of M-H^{a*} curve between H_{SF} and H_c and the zero-temperature value is obtained by the extrapolation. Thus, we have $dM^{a*}/dH(0) \approx 0.0065\ \mu_B$/kOe and $H_{SF}(0) = 12.68$ kOe. The anisotropy field is then estimated as $H_A = 0.2$ kOe and the exchange field $H_E = 387.8$ kOe from eqs 9 and 11. If the zero-field splitting alone contributes to the anisotropy field H_A, the zero-field parameter $|D|$ is estimated to be 0.005 cm^{-1} by using $g\mu_B H_A = 2|D|(S - 1/2)$. The ratio $\alpha = H_A/H_E$, a relative measure of the ideality of the isotropic exchange interaction, is estimated to be 5×10^{-4}. From eq 10, the critical field $H_c'(0)$ is estimated as $H_c'(0) = 775.8$ kOe. With equation $H_E = z|J|S/g\mu_B$, we can also get the intralayer exchange coupling $J = -3.61$ cm^{-1}, which is in good agreement with the values obtained before. One should notice the treatment on the spin-flop transition may not be fully applicable due to the hidden spin-canting and the values we have are of somewhat uncertainty.

When the applied field is along the *c* direction, perpendicular to the easy-axis *a** and the net moment along *b*, there is simply a smooth boundary separating the **AF** and **P** phases. This is the reason that there is no observed spin-flop phase transition along *c*.

Spin Configuration. Now it is possible to propose a reasonable picture of the spin arrangement that is consistent with the present structural and magnetic results, although neutron diffraction study is needed to confirm this picture. These results have revealed a two-dimensional spin system. Such spin arrangements before and after the critical fields applied along the a^* and b directions are depicted in Figure 12. In the AF state before the transition, the spins in each layer align almost along a^* with a small canting angle γ about 0.4°, which is enlarged in the figure for clarity, leading to a small net moment along b. The AF coupling between the layers causes the antiparallel of the net moments in adjacent layers and thus leads to the AF ground state. When the external field is along the b axis, a certain field overwhelms the interlayer AF coupling, rotates 180° all spins of one layer, and leads to a metamagnetic transition from the AF to the WF state. On the other hand, when the external field is along the a^* direction, which is parallel to the spin arrangements in the AF state, the spins flop from the a^* direction to the bc plane to be perpendicular to the external field.

Conclusions

In this paper, we reported the synthesis, the crystal structure and the detailed magnetic properties of the compound $Mn(N_3)_2(Btr)$ **1**. It is of (4,4) layers bridged by EE azides. We observed the combination of the spin-canting, the metamagnetism, and the spin-flop phenomena in this material. Below the Neél temperature 23.7 K, **1** behaves as an antiferromagnet with a hidden spin-canting. The spins are along the a^* axis with a small net moment toward the b axis in each bc layer. The net moments in adjacent layers are antiparallelly aligned by the interlayer AF coupling J^{a^*}. External fields along b can successfully overwhelm J^{a^*} and turn the system to a WF state through a first-order metamagnetic transition. On the other hand, the fields along a^* can induce a spin-flop transition. Careful magnetic measurements upon single crystal of **1** enable us to give the magnetic phase diagrams in both the $T-H^{a^*}$ and the $T-H^{b}$ planes and suggest the magnetic structures before and after the transitions below T_N. The origin of the hidden spin-canting is proved to be the antisymmitric superexchange interaction (DMI). The exchange field (H_E), the anisotropy field (H_A), the intralayer coupling (J), the interlayer exchange coupling (J^{a^*}), and the anisotropy parameter (α) are estimated to be $H_E = 387.8$ kOe, $H_A = 0.2$ kOe, $J = -3.35(1)$ cm^{-1}, $J^{a^*} = 6 \times 10^{-4}$ cm^{-1}, and $\alpha = 5 \times 10^{-4}$, respectively. Our data show that **1** is a good example of the 2D Heisenberg magnetic system.

Although the detailed magnetic measurements on the single crystal of **1** have given a lot of credible results of its magnetic properties, there still remains a lot to do. The heat capacity, the EPR, and the neutron diffraction on a single crystal are needed to fully characterize the phase transitions and exactly determine the magnetic structures. Works along these directions are now under the way.

Acknowledgment. We acknowledge support from the National Science Fund for Distinguished Young Scholars (20125104); NSFC Grants 20490210, 90201014, and 20221101; the National Basic Research Program of China (2006CB601102); and the Chun Tsung Fund of Peking University.

Supporting Information Available: Crystallographic data (CIF) of **1**. This material is available free of charge via the Internet at http://pubs.acs.org.

CM0521830